Magnetic catalysis (and inverse catalysis) at finite temperature in two-color lattice QCD

E.-M. Ilgenfritz

Joint Institute for Nuclear Research, VBLHEP, 141980 Dubna, Russia

M. Müller-Preussker, B. Petersson, and A. Schreiber

²Institut für Physik, Humboldt-Universität zu Berlin, 12489 Berlin, Germany
(Received 27 November 2013; published 24 March 2014)

Two-color lattice QCD with $N_f = 4$ staggered fermion degrees of freedom (no rooting trick is applied) with equal electric charge q is studied in a homogeneous magnetic background field B and at nonzero temperature T. In order to circumvent renormalization as a function of the bare coupling, we apply a fixed-scale approach. We study the influence of the magnetic field on the critical temperature. At rather small pseudoscalar meson mass $[m_\pi \approx 175 \text{ MeV} \approx T_c(B = 0)]$ we confirm a monotonic rise of the quark condensate $\langle \bar{\psi}\psi \rangle$ with increasing magnetic field strength, i.e., *magnetic catalysis*, as long as one is staying within the confinement or deconfinement phase. In the transition region we find indications for a nonmonotonic behavior of $T_c(B)$ at low magnetic field strength ($qB < 0.8 \text{ GeV}^2$) and a clear rise at stronger magnetic field. The conjectured existence of a minimum value $T_c(B^*) < T_c(B = 0)$ would leave a temperature window for a decrease of $\langle \bar{\psi}\psi \rangle$ with rising B (*inverse magnetic catalysis*) also in the present model.

I. INTRODUCTION

The interaction of strong magnetic fields with hadronic matter has recently been widely discussed because of its relevance to noncentral heavy-ion collisions. In such collisions there are two lumps of spectators moving in opposite directions. They give rise to a magnetic field perpendicular to the reaction plane, which may be estimated from the Lienard-Wiechert potentials of the moving spectators. From these estimates it can be shown that the magnetic field is so strong that its consequences cannot be studied perturbatively. In fact, the field is estimated to have strength $eB \sim m_\pi^2 \sim 10^{18}$ Gauss at the Relativistic Heavy-Ion Collider (RHIC) and at the Large Hadron Collider (LHC) at the time of the formation of the fireball. The field strength falls for large time t at most as $1/t^2$ and because of the effect of electrical conductivity may reach a plateau [1–3]. Therefore, for a longer time reaching from the formation of the fireball to the final transition from quark-gluon to hadron matter, it may be a reasonable approximation to assume a constant external field exerting influence on the transition.

It has been known for a long time that the problem of a relativistic particle with spin 0 or 1/2 in a constant external magnetic field can be solved exactly [4–6]. With the help of these solutions one can discuss the effect in the Nambu-Jona-Lasinio [7] or in the chiral [8] model at zero temperature. The general result is that the magnetic field induces an increase of the chiral condensate. This was dubbed *magnetic catalysis* in Ref. [9] and claimed to be essentially model independent. For a recent review, see [10]. The model calculations have been extended to finite

temperature in order to study the phase diagram of strongly interacting matter in a constant magnetic field. In this case there is no claim of model independence. The critical temperature of the chiral phase transition rises in most calculations [11]. There are also claims that the chiral and the deconfinement phase transitions split, and the latter decreases with the magnetic field strength [12].

Recently several groups have started to investigate the problem through ab initio lattice simulations of QCD and QCD-like theories in a constant external magnetic field. There is no sign problem in contrast to e.g. the introduction of a chemical potential in QCD. The pioneering work was performed by M. Polikarpov and collaborators [13–16]. They carried out their calculations in quenched $SU(2)$. In our previous paper [17] we extended the calculations to $SU(2)$ with four flavors of dynamical fermions. The choice of four flavors eliminates the need for rooting of the Kogut-Susskind or staggered fermion action, the latter being still under debate. One should notice that in this case we expect a first-order finite temperature transition [18] in contrast to the observed smooth crossover in the $N_f = 2$ as well as $2 + 1$ cases of full QCD at nonvanishing u-, d-quark mass. In Ref. [17] we reported magnetic catalysis for all temperatures investigated. The deconfinement transition, which we determined from the behavior of the Polyakov loop and the various parts of the gluonic action, coincided within our precision with the chiral transition. The transition temperature increased with increasing magnetic field. However, in our previous calculations the temperature dependence was studied only by varying the bare coupling parameter β, while the magnetic field strength as well as the fermion

mass was fixed in lattice units. As a consequence the physical field strength as well as the fermion mass was increasing with the temperature. This disadvantage is avoided in our present paper.

Two groups have performed simulations in full QCD in the presence of a magnetic field ([19–21] and [22–26], see also [27]). Both groups observe magnetic catalysis for temperatures in the confined phase. Near the phase transition only the second group observes what they call *inverse magnetic catalysis*; i.e., the chiral condensate and thus the transition temperature decrease with increasing magnetic field strength [22]. It is still not completely clear whether the discrepancy is explained by the different sets of quark masses used. In [20], the case of two flavors is treated, and the parameters chosen lead to a pion mass of approximately 200 MeV. In [22], the parameters and the action used are the same as in [28], namely 2 + 1 flavors with the parameters chosen to give the physical mass to the Goldstone pion connected to the exact lattice axial symmetry $U(1)$. In both calculations, the fourth root of the fermion determinants is taken to reduce the number of flavors (also called tastes). This procedure is still under debate. A nice recent review of the lattice results for QCD and QCD-like theories in external fields can be found in Ref. [29].

In this article we extend our calculations in [17] of the two-color theory with four-flavor fermion degrees of freedom with equal electric charges to a considerably smaller value of the bare quark mass. In fact, now the ratio of the Goldstone pion mass to the critical temperature is similar to the physical case of QCD. Furthermore, we use the fixed-scale approach, which means that the lattice spacing dependence of the renormalization factors is irrelevant for our results. We measure the various parts of the gluon action, the Polyakov loop and the chiral condensate. With the help of these measurements, we localize the finite temperature transition and describe its dependence on the magnetic field strength. Although our model is not QCD, the chiral properties are quite similar. Furthermore, investigations of the dynamic $SU(2)$ theory are of considerable interest because they can be extended to finite chemical potential without a sign problem. It is also easier to investigate the topologic structure of the lattice gauge fields than in the $SU(3)$ case.

In Sec. II, for completeness, we specify the action and the order parameters, although they are the same as in our previous calculation [17]. In Sec. III we describe the simulation parameters and in Sec. IV the scale determination. Section V is devoted to a presentation of our finite temperature results. Finally, in Sec. VI, we discuss the results, compare with results of other groups, and present our conclusions.

II. SPECIFICATION OF THE ACTION AND ORDER PARAMETERS

The theory, which we have chosen to investigate, is color $SU(2)$ with four fermion flavors. We want to study its behavior at finite temperature under the influence of a strong external magnetic field. To this end we perform numerical simulations in the lattice regularization, which are fully nonperturbative also in the electromagnetic coupling to the magnetic field. The details of the corresponding model on the lattice are given in [17]. For completeness we present again the main building blocks here.

We introduce a lattice of four-dimensional size

$$\mathcal{V} \equiv N_\tau \times N_\sigma^3. \tag{1}$$

The sites are enumerated by $n = (n_1, n_2, n_3, n_4)$, where the n_i are integers, $n_i = 1, 2, \ldots, N_\sigma$ for $i = 1, 2, 3$ and $n_4 = 1, 2, \ldots, N_\tau$. The fourth direction is taken as the Euclidean time direction. The lattice spacing is denoted by a. The physical volume V and the temperature T of the system are given by

$$V = (aN_\sigma)^3, \tag{2}$$

$$T = \frac{1}{aN_\tau}. \tag{3}$$

On the links $n \to n + \hat{\mu}$ we define group elements $U_\mu(n) \in SU(2)$, where $\mu = 1, 2, 3, 4$. The boundary conditions of the U fields are periodic. For the gauge part of the action we choose the usual Wilson action,

$$S_G = \beta \mathcal{V} \sum_{\mu < \nu} P_{\mu\nu}, \tag{4}$$

where

$$P_{\mu\nu} = \frac{1}{\mathcal{V}} \sum_n \left(\frac{1}{2} \times \mathrm{Tr}(1 - U_{\mu\nu}(n)) \right), \tag{5}$$

with $U_{\mu\nu}(n)$ denoting the $\mu\nu$-plaquette matrix attached to the site n.

For the fermion part of the action, we use staggered fermions, which are spinless Grassmann variables $\bar{\psi}(n)$ and $\psi(n)$ being vectors in the fundamental representation of the gauge group $SU(2)$. The different flavor degrees of freedom are assumed to carry equal electric charges allowing interaction with an external magnetic field. The boundary conditions of the fermionic fields are periodic in the space directions and antiperiodic in the time direction. In the absence of a magnetic field, the fermionic part of the action which we use becomes the usual staggered action,

$$S_F = a^3 \sum_{n,n'} \bar{\psi}(n)[D(n,n') + ma\delta_{n,n'}]\psi(n'), \tag{6}$$

where ma is the bare quark mass and

$$D(n,n') = \frac{1}{2} \sum_\mu \eta_\mu(n)[U_\mu(n)\delta_{n+\mu,n'} - U_\mu^\dagger(n-\mu)\delta_{n-\mu,n'}]. \tag{7}$$

The arguments n, n' are integer 4-vectors denoting sites on the lattice, and $\eta_\mu(n)$ are the normal staggered sign factors,

$$\eta_1(n) = 1,$$
$$\eta_\mu(n) = (-1)^{\sum_{\nu=1}^{\mu-1} n_\nu},$$
$$\mu = 2, 3, 4. \quad (8)$$

We introduce electromagnetic potentials in the fermion action by new, commuting group elements on the links, namely $V_\mu(n) = e^{i\theta_\mu(n)} \in U(1)$. As discussed in our earlier work [17], a constant magnetic background field in the $z \equiv 3$ direction going through all of the $(x, y) \equiv (1, 2)$ planes of finite size $N_\sigma \times N_\sigma$ with a constant magnetic flux $\phi = a^2 qB$ through each plaquette can be realized as follows:

$$V_1(n) = e^{-i\phi n_2/2} \quad (n_1 = 1, 2, …, N_\sigma - 1),$$
$$V_2(n) = e^{i\phi n_1/2} \quad (n_2 = 1, 2, …, N_\sigma - 1),$$
$$V_1(N_\sigma, n_2, n_3, n_4) = e^{-i\phi(N_\sigma+1)n_2/2},$$
$$V_2(n_1, N_\sigma, n_3, n_4) = e^{i\phi(N_\sigma+1)n_1/2},$$
$$V_3(n) = V_4(n) = 1. \quad (9)$$

With periodic boundary conditions, the magnetic flux becomes quantized in units of $2\pi/N_\sigma^2$,

$$\phi = a^2 qB = \frac{2\pi N_b}{N_\sigma^2}, \qquad N_b \in Z. \quad (10)$$

Because the angle ϕ is periodic, there is an upper bound on the flux $\phi < \pi$. In practice, to avoid finite-size effects, we restrict ourselves to $\phi < \pi/2$. By inserting this into (10), one obtains the condition

$$N_b < N_\sigma^2/4. \quad (11)$$

Thus, at finite temperature, $\frac{\sqrt{qB}}{T}$ (for $qB > 0$) is restricted to the region

$$\sqrt{2\pi} \frac{N_\tau}{N_\sigma} \leq \frac{\sqrt{qB}}{T} < \sqrt{\frac{\pi}{2}} N_\tau. \quad (12)$$

Finally, we introduce the fields $V_\mu(\theta)$ into the fermionic action (7) by substituting

$$U_\mu(n) \rightarrow V_\mu(n) U_\mu(n), \quad (13)$$

$$U_\mu^\dagger(n) \rightarrow V_\mu^*(n) U_\mu^\dagger(n). \quad (14)$$

The partition function is given by

$$Z(\theta) = \int \prod (d\bar{\psi}(n) d\psi(n) dU_\mu(n)) e^{-S_G - S_F(\theta)}. \quad (15)$$

Note that the fields $\theta_\mu(n)$ are not treated as dynamical variables and that there is thus no corresponding dynamic part of the action.

To determine the lattice spacing, we calculate the potential between heavy quarks on a zero-temperature lattice at vanishing magnetic field. On the same lattice we also measure the Goldstone pion mass. Details of these calibration measurements are given in Sec. IV below.

To study the influence of an external magnetic field on two-color QCD at finite temperature, we first look at the anisotropy in the gluonic action by measuring the average value $\langle P_{\mu\nu} \rangle$ of the non-Abelian plaquette energies for the different combinations of directions.

We further measure the following approximate order parameters.

The chiral condensate, which is an exact order parameter in the limit of vanishing quark mass, is given by

$$a^3 \langle \bar{\psi}\psi \rangle = -\frac{1}{\mathcal{V}} \frac{1}{4} \frac{\partial}{\partial(ma)} \log(Z)$$
$$= \frac{1}{\mathcal{V}} \frac{1}{4} \langle \text{Tr}(D + ma)^{-1} \rangle. \quad (16)$$

The factor $1/4$ is inserted because we define $\langle \bar{\psi}\psi \rangle$ per flavor, and our theory has four flavors.

We compute also the average value of the Polyakov loop $\langle L \rangle$, which is the order parameter for the deconfinement transition in the limit of infinite quark mass (the pure gauge theory),

$$\langle L \rangle = \frac{1}{N_\sigma^3} \sum_{n_1, n_2, n_3} \frac{1}{2} \left\langle \text{Tr}\left(\prod_{n_4=1}^{N_\tau} U_4(n_1, n_2, n_3, n_4) \right) \right\rangle. \quad (17)$$

It is important to notice that the mean values defined above are bare quantities which should be renormalized when comparing with continuum expectation values.

III. SIMULATION SETUP

In the present investigation we use the fixed-scale approach; i.e., we keep β fixed and thereby the lattice spacing a and vary the temperature by changing N_τ. More precisely, we simulated the theory at $\beta = 1.80$ mainly with lattice sizes $32^3 \times N_\tau$, $N_\tau = 4, 6, 8, 10$ and with a lowest mass value $ma = 0.0025$ taking each time at least three values of the magnetic flux, $N_b = 0, 80, 200$.

The simulation algorithm employed is the usual Hybrid Monte Carlo method, updated in various respects in order to increase efficiency [even-odd and mass preconditioning, multiple time scales, Omelyan integrator, and written in CUDA Fortran for the use on graphic processing units (GPUs)]. The number of configurations (trajectories) generated in a simulation varied between 3000 and 5000. In general, 250 configurations were discarded for initial thermalization.

We measured the chiral condensate on every third configuration, apart from $N_\tau = 6$ and $N_b = 80, 200$, where we used every fifth configuration only, because in these runs we are close to the transition temperature. The

Polyakov loop and the plaquette variables were measured on every configuration. The chiral condensate was evaluated with the random source method. Thereby we used 100 Z_2 random sources per configuration. The integrated autocorrelation times of all observables were taken into account in the error analysis. It could be estimated to be mostly well below 20 consecutive trajectories.

A zero-temperature simulation with zero magnetic field was performed for the same $\beta = 1.80$ and for the two mass values $ma = 0.0025, 0.01$ on a lattice of size $32^3 \times 48$ in order to estimate the lattice spacing and the pion mass. The number of trajectories in this run was about 750, and the first 200 were discarded. Measurements were performed after every third trajectory.

IV. FIXING THE LATTICE SCALE

In order to determine the lattice spacing, we investigate the potential between infinitely heavy quarks. We use the Sommer parameter, defined in the continuum by the equation

$$r^2 \frac{dV}{dr}\bigg|_{r=r_0} = 1.65. \tag{18}$$

On the lattice, we measure the potential using Wilson loops. In order to increase the signal-to-noise ratio, hypercubic blocking (*HYP smearing*) [30] with additional APE smearing [31] (in the version used in [32]) was applied to the gauge configurations before measurements were performed. The potential $V(\vec{R})$ as extracted from Wilson loops is not spherically symmetric, in particular for small distances. Defining R as the distance in lattice units ($r = Ra$), we introduce a more symmetric potential $V_S(R)$ by [33,34]

$$V(\vec{R}) = V_S(R) + C\left(\frac{1}{R} - G_L(\vec{R})\right), \tag{19}$$

where $G_L(\vec{R})$ is the free gluon propagator on the lattice. We then make the Ansatz

$$V_S(R) = A_1 - \frac{A_2}{R} + \sigma a^2 R. \tag{20}$$

The potential $V_S(R)$ as well as the best fit is shown in Fig. 1 (left panel). The fit parameters are given in Table I. As the two sides in Eq. (18) are dimensionless, the same equation holds for the lattice distance R. Thus, assuming the form (20) for the potential V in (18), we obtain

$$r_0/a = R_0 = \sqrt{\frac{1.65 - A_2}{\sigma a^2}}. \tag{21}$$

We are, of course, aware of the fact that we are considering a fictitious world of two-color QCD with four flavors of quarks with equal charges q. Nevertheless, the scale determination provides a rough estimate of the magnetic field strength for the various values of the flux and the distance to the chiral limit.

By inserting the value $r_0 = 0.468(4)$ fm [35], we obtain the lattice spacing from a fit with the formula (21)

$$a = 0.168(4) \text{ fm} \tag{22}$$

for $ma = 0.0025$ and an only slightly larger value for $ma = 0.01$ [17] (see Table III). Through variation of the fit range, we estimate the systematic error of the lattice spacing to be smaller than 10%.

To determine the Goldstone pion mass, we calculate the corresponding correlator, which is given by

$$C(n_4) = \sum_{n_1,n_2,n_3} |G(n,0)|^2, \tag{23}$$

where $G(n,0)$ is the quark propagator on the lattice. We did not apply any smearing in this case. Although there are in principle benefits by using more complicated sources, we found that simple point sources are sufficient in our case. The effective mass
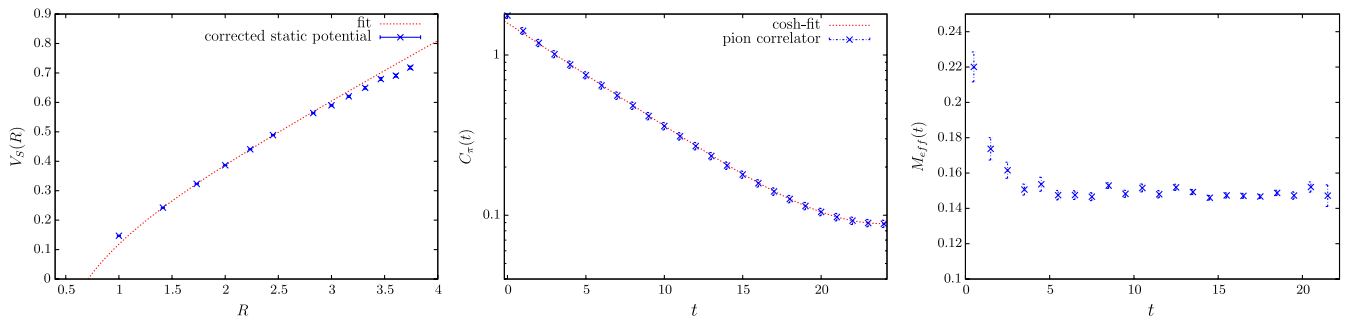

FIG. 1 (color online).   Potential of a static quark-antiquark pair (left), pion correlator (middle), and effective mass $M_{\text{eff}}(t)$ (right) all measured at $\beta = 1.80$ and bare quark mass $am = 0.0025$. The lattice size is $32^3 \times 48$. The dotted line in the left panel corresponds to a fit, the parameters of which are given in Table I.

TABLE I.   Fit parameters in lattice units for the static potential $V(\vec{R})$ according to Eqs. (19) and (20) for two sets of parameters considered in [17] and in this work. R_1 and R_2 define the fit range for the static potential in lattice units.

β	am	N_σ	N_τ	R_1	R_2	C	A_1	A_2	σa^2	χ^2_{dof}
1.8	0.01	16	32	1.2	3.2	0.167(25)	0.265(38)	0.370(42)	0.169(8)	0.87
1.8	0.0025	32	48	1.2	3.0	0.083(21)	0.078(24)	0.152(21)	0.192(7)	1.16

$$M_{\mathrm{eff}}\left(n_4 + \frac{1}{2}\right) = \log\frac{C(n_4)}{C(n_4 + 1)} \qquad (24)$$

was analyzed to determine the range where the contribution of higher states is negligible, corresponding to a plateau in $M_{\mathrm{eff}}(n_4)$ (see the middle and right panels of Fig. 1).

In the plateau range we measure the Goldstone pion mass from a fit to the correlator (23) of the form

$$C_\pi(t) = C_0(e^{-Et} + e^{E(t-N_\tau)}), \qquad (25)$$

where $t \equiv n_4$ and $E = m_\pi a$. We obtain a clear plateau in the effective mass and a very good fit for $t_{\mathrm{min}} = 7$, as can be seen in Table II.

Inserting the value of a from (22) in the result for E leads to

$$m_\pi = 175(4) \text{ MeV}, \qquad (26)$$

for $ma = 0.0025$ which is, as expected from the phenomenologic rule $m_\pi^2 \propto m_q$, about half the value obtained for $ma = 0.01$ [17] (cf. Table III). As we see below, we now have $m_\pi \approx T_c(B=0)$. Therefore, we expect that our results are relevant to the physical case of QCD.

V. RESULTS

We start by discussing the influence of the temperature and magnetic field on the different parts $P_{\mu\nu}$ of the gluonic action. For convenience, we introduce similar variables as in [25]:

$$\mathcal{E}_i^2 = \langle P_{4i}\rangle, \qquad (27)$$

$$\mathcal{B}_i^2 = |\epsilon_{ijk}|\langle P_{jk}\rangle, \qquad j < k. \qquad (28)$$

At $B = T = 0$ they are all equal by symmetry. At $B = 0, T \neq 0$ they fall into two groups because the fourth direction is not equivalent to the other ones:

$$\mathcal{E}_1^2 = \mathcal{E}_2^2 = \mathcal{E}_3^2 \leq \mathcal{B}_1^2 = \mathcal{B}_2^2 = \mathcal{B}_3^2. \qquad (29)$$

Introducing a magnetic field in the third direction, for $T \neq 0$ the only symmetries left are rotations in the (1,2) plane. We therefore may define

$$\mathcal{E}_\parallel^2 \equiv \mathcal{E}_3^2, \qquad (30)$$

$$\mathcal{E}_\perp^2 \equiv \mathcal{E}_1^2 = \mathcal{E}_2^2, \qquad (31)$$

$$\mathcal{B}_\parallel^2 \equiv \mathcal{B}_3^2, \qquad (32)$$

$$\mathcal{B}_\perp^2 \equiv \mathcal{B}_1^2 = \mathcal{B}_2^2. \qquad (33)$$

In Fig. 2, we show the results for the four values of the temperature T and each of them for the three values of the magnetic field qB. We give T and qB in physical units via Eq. (22).

We can see the following features from this figure. The pattern of the splitting is the same as in our earlier article [17] and is more recently found in full QCD [25],

TABLE II.   Fit parameters in lattice units for the pion correlator $C_\pi(t)$ according to Eq. (25) for the two sets of simulation parameters considered in [17] and in this work. The fit range for the pion correlator starts at lattice distance t_{min}.

β	am	N_σ	N_τ	t_{min}	C_0	$E = am_\pi$	χ^2_{dof}
1.8	0.01	16	32	6	1.01(3)	0.285(1)	0.023
1.8	0.0025	32	48	7	1.58(8)	0.149(3)	0.010

TABLE III.   Results for the Sommer scale R_0 (in lattice units), the lattice spacing a, the pion mass m_π, and the quantity $\sqrt{qB_m}$ characterizing the magnetic field strength for the largest number of flux units N_b^m used for various setups of simulation parameters considered in [17] and this work.

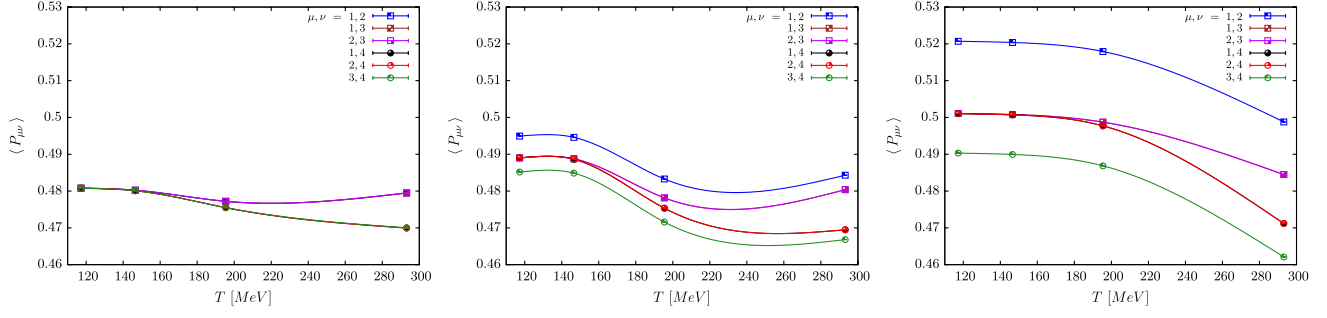| β	am	N_σ	N_τ	N_b^m	R_0	$a[\mathrm{fm}]$	$m_\pi[\mathrm{MeV}]$	$\sqrt{qB_m}[\mathrm{GeV}]$
1.8	0.01	16	32	50	2.75(8)	0.170(5)	330(10)	1.29(4)
1.8	0.0025	32	48	200	2.78(6)	0.168(4)	175(4)	1.30(3)

FIG. 2 (color online).   Plaquette energies $\langle P_{\mu\nu} \rangle$ versus temperature $T = (a(\beta)N_\tau)^{-1}$ without the magnetic field (left panel), with $qB = 0.67$ GeV^2 (middle) and $qB = 1.69$ GeV^2 (right panel) for the different plaquette orientations. The lines are only to guide the eye. Computations were done for $\beta = 1.80$, $am = 0.0025$, $N_\sigma = 32$.

$$\mathcal{B}_{\parallel}^2 \geq \mathcal{B}_{\perp}^2 \geq \mathcal{E}_{\perp}^2 \geq \mathcal{E}_{\parallel}^2. \tag{34}$$

The difference $\delta_{\perp} \equiv \mathcal{B}_{\perp}^2 - \mathcal{E}_{\perp}^2$ is proportional to a gluonic contribution to the entropy density of the system (see e.g. [36,37]). Although the latter is not an order parameter, it is a good indicator for the transition into the deconfinement phase. It increases as one gets deeper into the deconfinement phase. In Fig. 2, we may compare the $\delta_{\perp}$ values at fixed $N_\tau = 6$ [i.e. $T = 195$ MeV $\gtrsim T_c(B=0)$] for the three different qB values represented in the three panels. We find the relations $\delta_{\perp}(qB = 0.67 \, \text{GeV}^2) > \delta_{\perp}(qB = 0) > \delta_{\perp}(qB = 1.69 \, \text{GeV}^2)$. We take this as a first hint for a nonmonotonous behavior of the transition temperature: $T_c(qB=0.67\,\text{GeV}^2) < T_c(B=0) < T_c(qB= 1.69\,\text{GeV}^2)$. We return to a discussion of plaquette observables as a function of qB at the end of this section.

In Fig. 3 (left), the expectation value of the unrenormalized Polyakov loop $\langle L \rangle$ is shown as a function of the temperature. Our values $N_\tau = 10$, 8, 6, 4 correspond to temperature values T, which are quite widely spaced. Therefore, we cannot localize the transition, e.g., for $B = 0$, very well. It happens around $T = T_c \simeq 160 - 190$ MeV.

This means that $T_c \simeq m_\pi$, like in QCD. We observe again an interesting pattern at $T = 195$ MeV ($N_\tau = 6$), namely that also the Polyakov loop does not behave monotonously with the magnetic field (observed already in Refs. [17,19]). We come back to that behavior later. We are aware of the fact that a proper renormalization of the Polyakov loop with respect to the N_τ dependence will weaken the steep rise with T. However, our main conclusions concerning the qB dependence at fixed T values remain unchanged.

In Fig. 3 (right), the unrenormalized chiral order parameter $a^3 \langle \bar{\psi}\psi \rangle$ is shown versus T. We observe that for a fixed nonvanishing quark mass it grows monotonously with the magnetic field at least for the three lower temperature values we have investigated. This could be interpreted as compatible with an overall magnetic catalysis. However, at $T = 195$ MeV, i.e. slightly above $T_c(B=0)$, we detect a strong rise of the condensate between $qB = 0.67$ GeV^2 and our largest value 1.69 GeV^2, while between $qB = 0$ and $qB = 0.67$ GeV^2 only a small increase of $\langle \bar{\psi}\psi \rangle$ is observed. This behavior shows that the system with rising magnetic field strength remains in the chirally symmetric
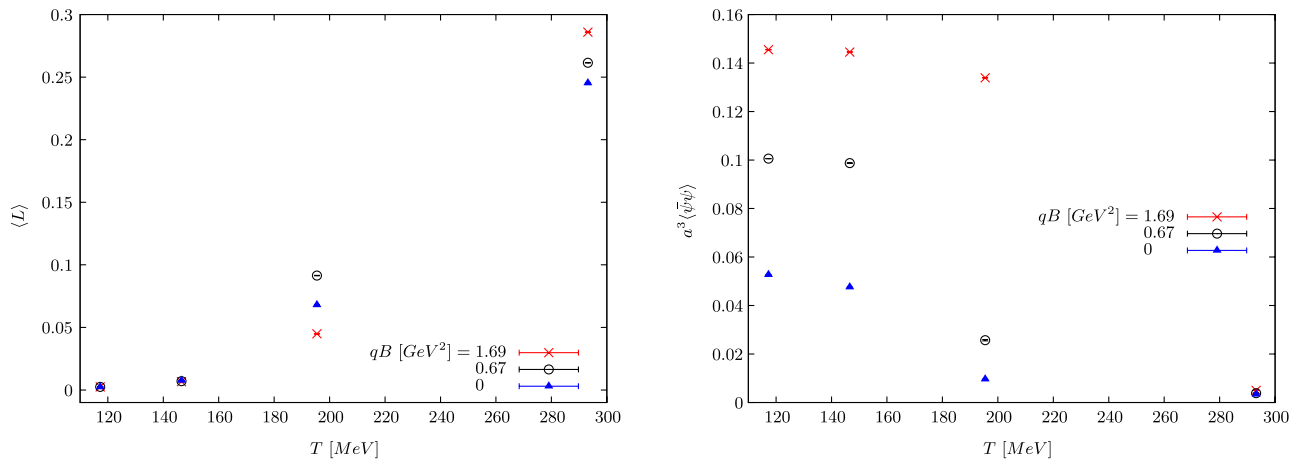

FIG. 3 (color online).   Bare Polyakov loop $\langle L \rangle$ (left) and bare chiral condensate $\langle \bar{\psi}\psi \rangle$ (right) versus temperature $T = (a(\beta)N_\tau)^{-1}$ shown for three values of the magnetic field strength at $\beta = 1.80$, $am = 0.0025$ and lattice sizes $32^3 \times N_\tau$, $N_\tau = 4$, 6, 8, 10.
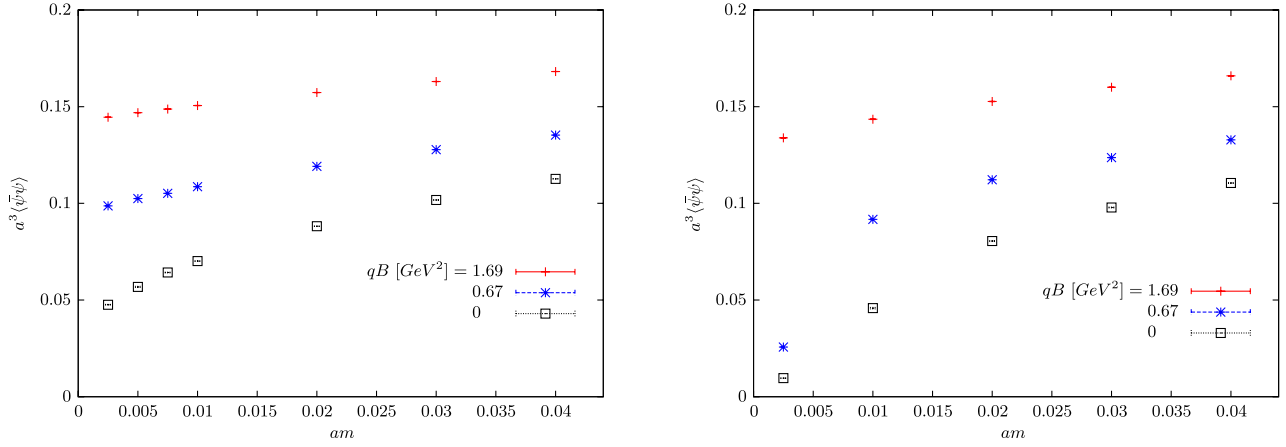
FIG. 4 (color online).   Mass dependence of the bare chiral condensate $\langle \bar{\psi}\psi \rangle$. Data points are shown for $N_\tau = 8$, i.e. $T = 147$ MeV (left panel) and for $N_\tau = 6$, i.e. $T = 195$ MeV (right panel), in each case for three values of the magnetic field. The simulations were done with $\beta = 1.80$ and spatial linear lattice extent $N_\sigma = 16$, except for the three smallest mass values $am = 0.0025, 0.0050, 0.0075$, where $N_\sigma = 32, 24, 20$, respectively, was chosen.

phase until it suddenly jumps back into the chirally broken phase, when the magnetic field becomes strong enough. This indicates that $T_c(B)$ is rising for sufficiently high magnetic field strength. At weak magnetic fields, where we saw indications for a lowering of the critical temperature, the chiral condensate nevertheless does not decrease but increases, although much slower than at lower temperatures within the chirally broken phase.

We find this pattern confirmed in Fig. 4, where $a^3 \langle \bar{\psi}\psi \rangle$ is shown as a function of the bare quark mass ma at two temperatures, $T = 147$ and 195 MeV, respectively. One may use these data to extrapolate $a^3 \langle \bar{\psi}\psi \rangle$ down to the chiral limit. For $T = 147$ MeV (left panel), the system is clearly in the chirally broken phase for all values of B, including $B = 0$. At the higher temperature $T = 195$ MeV (right panel), the condensate $a^3 \langle \bar{\psi}\psi \rangle$ nicely extrapolates to zero for $qB = 0$ corresponding to the chirally restored phase. At the intermediate value $qB = 0.67$ GeV^2, there seems to be

a change of the regime at mass values below $am = 0.01$, such that the system is consistent with being in the chirally restored phase also at this magnetic field strength. On the other hand, for the strongest magnetic field strength 1.69 GeV^2, the data suggest a nonvanishing chiral condensate in the chiral limit. Thus, we may conclude that at very strong magnetic fields the transition temperature grows with B, while at fixed $T > T_c(B = 0)$, the chiral condensate is strongly rising, when the system passes over to the chirally broken phase. This is compatible with magnetic catalysis in agreement with various models [10].

In order to study the situation in more detail, we have made simulations at fixed $T = 195$ MeV ($N_\tau = 6$) with a few more values of N_b. The latter correspond to a range of qB between 0 and 1.69 GeV^2. We again measure the expectation values of the Polyakov loop and the chiral condensate. The results are shown in Fig. 5. There is a sharp change, which might be related to a phase transition
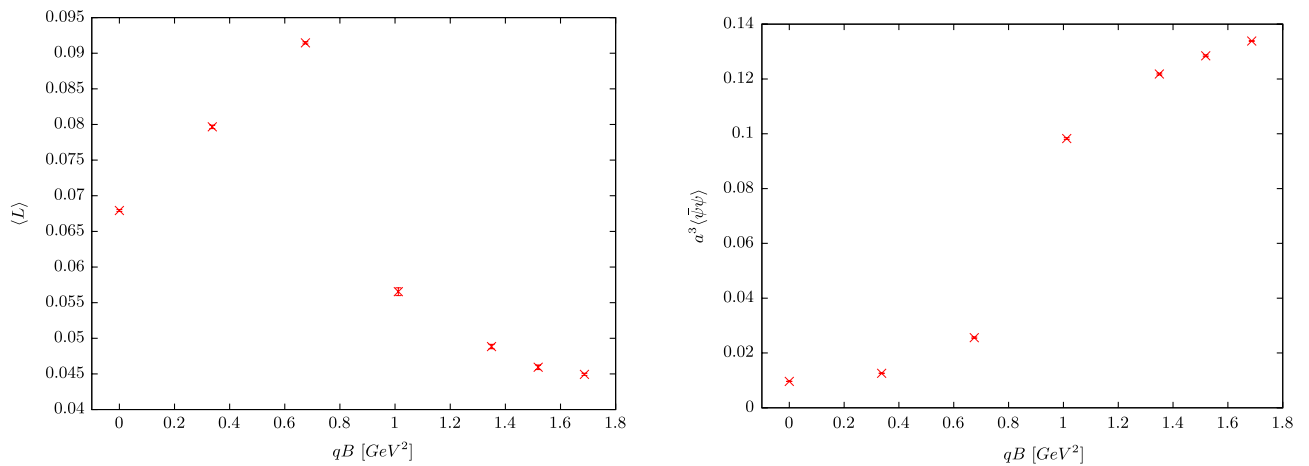

FIG. 5 (color online).   Polyakov loop (left panel) and chiral condensate (right panel) vs field strength qB at $T = 195$ MeV obtained with $\beta = 1.80$, $am = 0.0025$ and lattice size $32^3 \times 6$.
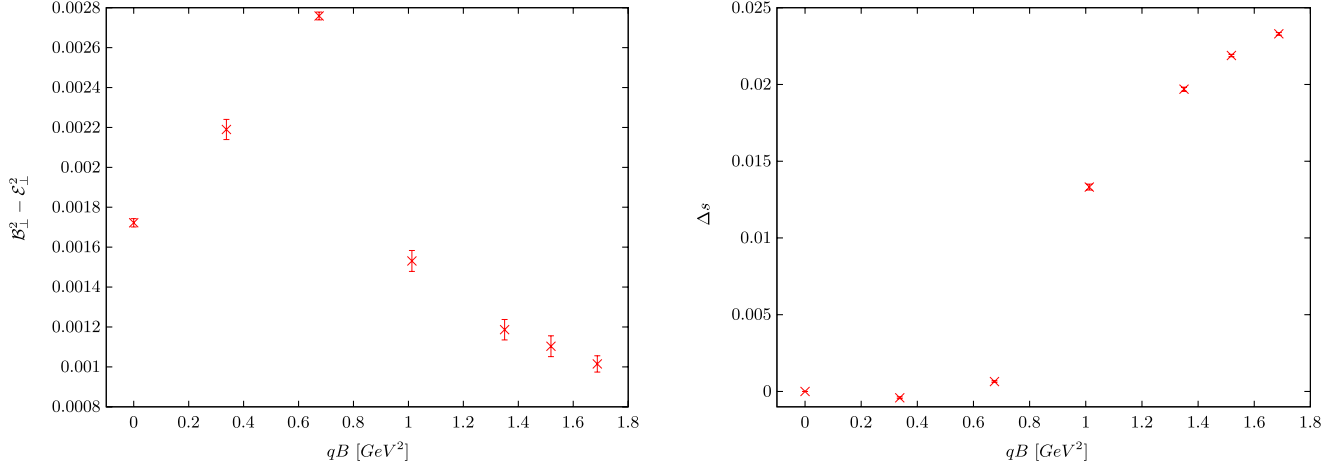
FIG. 6 (color online).   The difference of plaquette energies $\delta_\perp = \mathcal{B}_\perp^2 - \mathcal{E}_\perp^2$ (left panel) as well as the purely gluonic contribution Δs to the interaction measure (right panel) versus field strength qB at $T = 195$ MeV, as in Fig. 5.

in the range 0.7 GeV$^2 < qB < 1.0$ GeV^2 corresponding to $\sqrt{qB}/T \approx 4.5$. This observation is again supporting a magnetic catalysis phenomenon. For lower magnetic fields, we observe a rise of the Polyakov loop with qB toward the transition and only then a dropoff followed by a monotonous decrease at larger field values [compare with our previous comment to Fig. 3 (left)]. The rise at low magnetic field values suggests that we are going deeper into the deconfinement region, after which the transition brings us back into the confinement or chirally broken phase. The observation of the rise of the Polyakov loop at low magnetic field values resembles the pattern discussed in Refs. [26], where it was related to the inverse magnetic catalysis phenomenon.

The reader should keep in mind that these data are all obtained at fixed quark mass $am = 0.0025$. There the chiral condensate (see the right panel of Fig. 5) rises also at a weak field qB. However, in this deconfinement range, which should be separated from the chirally broken phase by a first-order transition, the chiral condensate is anyway expected to vanish in the chiral limit. Therefore, the weak monotonous rise of the chiral condensate with qB at the given temperature $T > T_c(B = 0)$ does not mean that an inverse magnetic catalysis cannot occur in our model at sufficiently small quark mass.

In order to gain more information, let us come back to the plaquette variables. In Fig. 6 (left), we show the plaquette energy difference $\delta_\perp = \mathcal{B}_\perp^2 - \mathcal{E}_\perp^2$ as a function of qB for the same temperature as in Fig. 5. Where we saw a rise of the Polyakov loop with qB, we observe now also a rise of the difference $\delta_\perp$, indicating again that we are going deeper into the deconfinement phase. Contrary to that, $\delta_\perp$ decreases at larger qB values, where we are driven by the magnetic field into the confinement phase. Another observable derived from the average plaquette variables is the gluonic contribution to the subtracted *interaction measure* defined as

$$\Delta s \equiv \langle P \rangle (T, B) - \langle P \rangle (T, B = 0), \qquad (35)$$

where $\langle P \rangle$ includes the average overall plaquette orientations. We do not consider a factor given by the derivative of the β function with respect to the lattice spacing because it is irrelevant in our fixed-scale method. We have plotted Δs versus qB in the right part of Fig. 6. At low values of qB, we observe a small decrease, whereas at larger magnetic field strength, Δs is rising. The decrease at low qB seems also to be compatible with a similar observation discussed in [25], where it was related to inverse magnetic catalysis.

Our observations above seem to indicate a decrease of T_c with rising but small qB. At large qB the transition temperature T_c definitely rises as expected in the case of magnetic catalysis. In Fig. 7, we conjecture a $B - T$ phase diagram, which might clarify the situation. In order to prove it, further simulations at somewhat smaller temperatures and/or smaller quark mass would be helpful. If it proves to be true, then for the same $am = 0.0025$ or even lower mass,
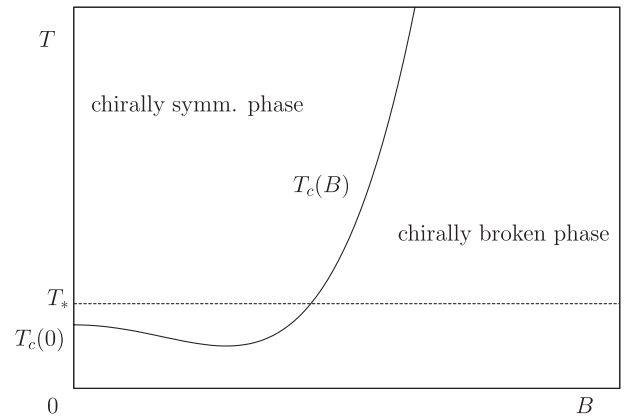

FIG. 7.   Conjectured B-T phase diagram at fixed mass $am = 0.0025$. The horizontal line indicates the path of simulations at $T = T_* = 195$ MeV, as in Figs. 5 and 6.

one should find another path $T = \text{const.} < T_c(B = 0)$, for which at $qB = 0$ the system is in the confinement (chirally broken) phase. With increasing qB one passes then the chirally restored phase, i.e., the deconfinement or chiral transition twice, and ends up again in the confinement phase. Along such a path in the phase diagram the chiral condensate should decrease with qB when entering the chirally restored phase. This would mean the existence of inverse magnetic catalysis also in two-color QCD.

Let us finally notice that in the recent papers [38,39] similar scenarios as proposed here were obtained for the cases $N_f = 2$ and $N_f = 2 + 1$, which differ from ours by a smooth crossover behavior.

VI. CONCLUSIONS

In this article we have described an investigation of two-color QCD at finite temperature in a constant external magnetic field. We specialized to the case of four flavors of equal charge q implementing staggered fermions on the lattice without employing the fourth root trick. We have performed lattice simulations using a fixed-scale approach so that we do not need to know the beta function and the dependence of the renormalization constants on the bare coupling constant. The simulations were carried out at a lattice spacing $a \approx 1/(6T_c(0))$, where $T_c(0)$ is the critical temperature of the finite temperature transition at vanishing magnetic field. Furthermore, we used a fixed bare quark mass which is four times smaller than in our previous work [17]. This means that now the Goldstone meson mass is $m_\pi \approx T_c(0)$ similar to the physical case of QCD. We have also taken some data at larger quark masses to be able to extrapolate to the chiral limit.

We find that at sufficiently large magnetic fields there is magnetic catalysis; i.e., the chiral order parameter and the critical temperature are increasing with increasing magnetic field strength. This is in agreement with predictions by many models. The result is, however, apparently different from that of Ref. [22] close to the physical point of QCD, where one finds inverse magnetic catalysis in the crossover region; i.e., the chiral order parameter is not increasing monotonically with the magnetic field strength, and as a consequence, the transition temperature decreases.

In our case of two-color QCD with $N_f = 4$ dynamic fermion degrees of freedom, a real phase transition is expected in contrast to a smooth crossover, and one may therefore expect that the deconfinement and chiral transition should coincide. Therefore, a priori an inverse magnetic catalysis phenomenon could be absent. However, as we showed, there are indications that for weak magnetic field the critical temperature $T_c(B)$ is decreasing with rising B. If so, for fixed sufficiently small quark mass and fixed

temperature $T \lesssim T_c(B = 0)$, we should be able to find a trajectory in the phase diagram along which one passes from the chirally broken phase with its large chiral condensate through the chirally restored phase with a suppressed chiral condensate again into the chirally broken phase at larger qB values. In this way we should observe a real inverse magnetic catalysis replacing the crossover behavior observed in QCD close to the physical point.

Since our theory is different from QCD, the behavior does not have to be the same, but the response of the system to a strong magnetic field should be to some extent model independent for theories with similar chiral properties. We note, however, that the magnetic field strength at which we see a clear signal of magnetic catalysis is (to the extent one can compare scales in different theories) larger than that investigated in [22]. At a magnetic field strength similar to those used in [22], our data are consistent with the possibility of an inverse magnetic catalysis scenario in the sense described above.

In [26], e.g., it is claimed that the inverse magnetic catalysis is due to the coupling of the magnetic field to the sea quarks. This also gives rise to an increase in the Polyakov loop with the magnetic field strength, which is an effect that we see in our calculations up to a critical magnetic field. Going beyond the latter, the Polyakov loop suddenly drops to a value near zero, and the system enters the confined phase. This critical magnetic field is stronger than that used in [22,26].

It would be very interesting to have results from QCD calculations at stronger magnetic fields to see if the phase diagram of [22] extends to the one we propose in Fig. 7 or if the inverse magnetic catalysis persists for all values of the magnetic field strength.

A further simulation of our model at a somewhat lower temperature would be helpful to pinpoint the critical line in the phase diagram. Investigations at different quark masses ma would be important because the phase transition line is expected to depend on the quark mass. Our calculations should be also extended to smaller scales a in order to extrapolate to the continuum limit.

[1] D. Kharzeev, L. McLerran, and H. Warringa, Nucl. Phys. **A803**, 227 (2008).

[2] V. Skokov, A. Illarionov, and V. Toneev, Int. J. Mod. Phys. A **24**, 5925 (2009).

[3] L. McLerran and V. Skokov, arXiv:1305.0774.

[4] J. Géhéniau, Physica (Utrecht) **16**, 822 (1950).

[5] Y. Katayama, Prog. Theor. Phys. **6**, 309 (1951).

[6] J. Schwinger, Phys. Rev. **82**, 664 (1951).

[7] S. Klevansky and R. Lemmer, Phys. Rev. D **39**, 3478 (1989).

[8] I. Shushpanov and A. Smilga, Phys. Lett. B **402**, 351 (1997).

[9] V. Gusynin, V. Miransky, and I. Shovkovy, Phys. Rev. Lett. **73**, 3499 (1994).

[10] I. A. Shovkovy, Lect. Notes Phys. **871**, 13 (2013).

[11] N. Agasian, Phys. At. Nucl. **64**, 554 (2001).

[12] N. Agasian and S. Fedorov, Phys. Lett. B **663**, 445 (2008).

[13] P. Buividovich, M. Chernodub, E. Luschevskaya, and M. Polikarpov, Phys. Lett. B **682**, 484 (2010).

[14] P. Buividovich, M. Chernodub, E. Luschevskaya, and M. Polikarpov, Nucl. Phys. **B826**, 313 (2010).

[15] P. Buividovich, M. Chernodub, E. Luschevskaya, and M. Polikarpov, Phys. Rev. D **80**, 054503 (2009).

[16] P. Buividovich, M. Chernodub, E. Luschevskaya, and M. Polikarpov, Phys. Rev. D **81**, 036007 (2010).

[17] E.-M. Ilgenfritz, M. Kalinowski, M. Müller-Preussker, B. Petersson, and A. Schreiber, Phys. Rev. D **85**, 114504 (2012).

[18] R. D. Pisarski and F. Wilczek, Phys. Rev. D **29**, 338 (1984).

[19] M. D'Elia, S. Mukherjee, and F. Sanfilippo, Phys. Rev. D **82**, 051501 (2010).

[20] M. D'Elia and F. Negro, Phys. Rev. D **83**, 114028 (2011).

[21] C. Bonati, M. D'Elia, M. Mariti, F. Negro, and F. Sanfilippo, Phys. Rev. Lett. **111**, 182001 (2013).

[22] G. S. Bali, F. Bruckmann, G. Endrődi, Z. Fodor, S. D. Katz, S. Krieg, A. Schäfer, and K. K. Szabó, J. High Energy Phys. 02 (2012) 044.

[23] G. Bali, F. Bruckmann, G. Endrődi, Z. Fodor, S. Katz, and A. Schäfer, Phys. Rev. D **86**, 071502 (2012).

[24] G. S. Bali, F. Bruckmann, M. Constantinou, M. Costa, G. Endrődi, S. D. Katz, H. Panagopoulos, and A. Schäfer, Phys. Rev. D **86**, 094512 (2012).

[25] G. Bali, F. Bruckmann, G. Endrődi, F. Gruber, and A. Schäfer, J. High Energy Phys. 04 (2013) 130.

[26] F. Bruckmann, G. Endrődi, and T. Kovacs, J. High Energy Phys. 04 (2013) 112.

[27] L. Levkova and C. DeTar, Phys. Rev. Lett. **112**, 012002 (2014).

[28] S. Borsányi, G. Endrődi, Z. Fodor, A. Jakovác, S. D. Katz, S. Krieg, C. Ratti, and K. K. Szabó, J. High Energy Phys. 11 (2010) 077.

[29] M. D'Elia, Lect. Notes Phys. **871**, 181 (2013).

[30] A. Hasenfratz and F. Knechtli, Phys. Rev. D **64**, 034504 (2001).

[31] M. Albanese *et al.* (APE), Phys. Lett. B **192**, 163 (1987).

[32] V. Bornyakov, E.-M. Ilgenfritz, and M. Müller-Preussker, Phys. Rev. D **72**, 054511 (2005).

[33] C. Michael, Phys. Lett. B **283**, 103 (1992).

[34] G. S. Bali and K. Schilling, Phys. Rev. D **47**, 661 (1993).

[35] A. Bazavov, T. Bhattacharya, M. Cheng, C. DeTar, H. Ding *et al.*, Phys. Rev. D **85**, 054503 (2012).

[36] J. Engels, F. Karsch, and K. Redlich, Nucl. Phys. **B435**, 295 (1995).

[37] G. Boyd, J. Engels, F. Karsch, E. Laermann, C. Legeland, M. Lütgemeier, and B. Petersson, Nucl. Phys. **B469**, 419 (1996).

[38] A. Amador and J. O. Andersen, Phys. Rev. D **88**, 025016 (2013).

[39] V. D. Orlovsky and Yu. A. Simonov, arXiv:1312.4178.